# Improvement of the Short-Fetch Behavior in the Wave Ocean Model (WAM)

H. HERSBACH

*Royal Netherlands Meteorological Institute, De Bilt, the Netherlands*

P. A. E. M. JANSSEN

*European Centre for Medium-Range Weather Forecasts, Reading, United Kingdom*

(Manuscript received 11 September 1996, in final form 5 August 1998)

ABSTRACT

The physics of wind input in the Wave Ocean Model (WAM) cycle 4 is based on scaling with the friction velocity $u_*$. This implies that in the case of fetch-limited wind-wave growth, universal scaling laws should follow if fetch and wave variance are scaled by means of $u_*$. For operational applications, such as at the European Centre for Medium-Range Weather Forecasts, the scaling of the WAM model with $u_*$ is well satisfied. Recently, however, it was found that this scaling is violated for very short waves at small fetches and durations, for which the model is run with very small grid spacings, a very small time step, and a large cutoff frequency. This violation of $u_*$ scaling, which is a serious problem for implementation on a small lake, was found to be caused by a too severe limit on the increments of the wave spectrum per time step. In this article, an alternative formulation for the limitation of spectral component growth is suggested, which does not violate $u_*$ scaling and, in addition, gives rise to excellent results over a large range of scaled quantities. At the same time, growth curves for wave height and peak frequency hardly depend on the time step.

## 1. Introduction

The Wave Ocean Model (WAM) (for a detailed description see Komen et al. 1994; WAMDI 1988) solves the energy balance equation for the wave spectrum $F$. Leaving out the advection terms, the evolution equation for $F$ reads

$$\frac{\partial F}{\partial t} = S, \tag{1}$$

where $S$ is a source term consisting of wind input, nonlinear interactions, and dissipation. The energy balance of the wave spectrum is evaluated in detail up to a high-frequency cutoff frequency $f_c$. (In operational applications, the frequency range is normally between 0.04 and 0.4 Hz.) The high-frequency adjustment timescales are considerably shorter than the evolution timescales of the energy-containing frequency bands near the peak of the spectrum. In this study we are interested in them mainly in terms of modeling applications. Thus, in the high-frequency region, it is sufficient to determine the quasi-equilibrium level to which the spectrum adjusts in response to the more slowly changing low-frequency waves. The time history of the short-time scale adjustment process, itself, does not need to be determined.

In WAM this was achieved by using a semi-implicit numerical integration scheme in which the time step matches the timescale of the low-frequency waves. If the source function $S$ has a stable fixed point, then the semi-implicit scheme can be shown to be numerically stable (Janssen et al. 1997). This is provided that we retain the full functional derivative of the source term $S$ with respect to the spectrum $F$, which is a two-dimensional matrix. In practice, we retain only the diagonal part of the functional derivative matrix. As a consequence, however, numerical stability is not guaranteed. To ensure numerical stability, a growth spectrum limit was added to WAM. Initially this growth limiter was independent of the integration time step. This resulted in a sensitive time-step dependence on the numerical results (Tolman 1992). Removal of the time-step dependence was achieved by proposing a time-step-dependent wave-growth limiter. This limiter was introduced in cycle 4 of WAM, which, in September 1991, became the operational wave forecasting model at the European Centre for Medium-Range Weather Forecasts (ECMWF). For operationally feasible resolutions ($\Delta x > 50$ km), satisfactory results were obtained. In this article, however, it will be shown that for very high resolution—relevant for applications in lakes, for example—the WAM cycle 4 limiter violates the well-

*Corresponding author address:* Dr. Hans Hersbach, Royal Netherlands Meteorological Institute (KNMI), P.O. Box 2013730 AE Utrecht, the Netherlands.
E-mail: hersbach@knmi-nl

known fetch-limited growth law for significant wave height.

In this article, a revised formulation of the cycle 4 limiter will be introduced. In addition, the reasons why it was chosen to depend on the friction velocity will be explained. Also, the new limiter, which is far less restrictive than the previous one, will be applied to the case of high spatial resolution (up to 1 km). Additionally, an experiment with a global application of WAM is performed. Although in the high resolution case the new limiter gives dramatic improvements, in the global application differences are seen only occasionally in rapidly varying circumstances near the coasts.

## 2. The semi-implicit integration scheme

WAM uses a semi-implicit scheme whose time step is matched to the evolution of the lower-frequency waves. For low-frequency waves, this integration method yields essentially the same results as a simple forward integration scheme (but it is of second order rather than first order), while for high-frequency waves, it yields the slowly changing quasi-equilibrium spectrum.

The semi-implicit difference equations are given by

$$F_{n+1} = F_n + \Delta t[(1 - \alpha)S_n + \alpha S_{n+1}], \qquad \alpha = \frac{1}{2}, \quad (2)$$

where $\Delta t$ is the time step and the index $n$ refers to the time level. Unfortunately, $S_{n+1} = S(F_{n+1})$ depends nonlinearly on the spectrum. Hence, we cannot solve directly for $F_{n+1}$. Therefore, $S_{n+1}$ was expanded around $F_n$; that is, a change $\Delta F_n = F_{n+1} - F_n$ will lead to a modified source $\Delta S_n = S_{n+1} - S_n$, which can be expanded by

$$\Delta S_n(x) = \int_y \left[\frac{\partial S(x)}{\partial F(y)}\right]_{F=F_n} \Delta F_n(y)\, dy + \cdots,$$

$$x, y \equiv (\mathbf{r}, f, \theta),$$

where $f$ is the frequency and $\theta$ is the direction of a plane wave, which is located around position $\mathbf{r}$. In a discretized form ($N$ degrees of freedom), the functional derivative $\partial S/\partial F$ reduces to an $N \times N$ dimensional matrix, and the integral reduces to a finite sum. In practice, only the diagonal term is retained, and only when it is negative:

$$S_{n+1} = S_n + \min\left(\frac{\partial S}{\partial F}, 0\right)(F_{n+1} - F_n) + \cdots, \quad (3)$$

in which case one can solve (2) directly for $F_{n+1}$:

$$F_{n+1} = F_n + \frac{\Delta t S_n}{1 - \min[\alpha \Delta t(\partial S/\partial F), 0]}. \quad (4)$$

The positive diagonal term is omitted for reasons of stability, which may be clear from (4).

## 3. Scale invariance

WAM is based on scaling with friction velocity $u_*$. This comes from the belief that as long as viscosity is not important the physics of ocean waves obeys a scale invariance. For instance, in the case of a fully developed wind sea it is expected that the significant wave height $H_s$ will be four times as large when the wind forcing, that is, $u_*$ (rather than $U_{10}$), is doubled. Therefore, $H_s$ can be factored into a dimensionless quantity $H_s^*$, a dimension-carrying factor containing $u_*$, and the gravitational acceleration $g = 9.81$ m s$^{-2}$:

$$H_s = H_s^*\left(\frac{u_*^2}{g}\right), \quad (5)$$

in which, according to Pierson and Moskowitz (1964), $H_s^* \sim 130$.

Such a decomposition can be made for any physical quantity. For the wave spectrum $F = F(\mathbf{r}, f, \theta)$, position $\mathbf{r}$, frequency $f$, and time $t$, a dimensional analysis leads directly to

$$F = F^*\left(\frac{u_*^5}{g^3}\right), \qquad \mathbf{r} = \mathbf{r}^*\left(\frac{u_*^2}{g}\right), \qquad f = f^*\left(\frac{g}{u_*}\right),$$

$$\text{and} \quad t = t^*\left(\frac{u_*}{g}\right). \quad (6)$$

The laws of ocean-wave evolution can be written in terms of dimensionless quantities only. For a specific application, this means that when we double all frequencies, halve all timescales and $u_*$, and divide all length scales by a factor of 4, the system remains equivalent, from a scaled point of view. Therefore, the evolution of $H_s^*$ will be identical, which results in four times as many low waves.

This should also be true for WAM. It is also true that a proper rescaling of the time and space discretization must lead to an identical finite difference scheme.

## 4. The limitation on wave growth

### *a. Numerical versus physical limitation*

In practice, it turned out that the resulting numerical scheme incorporated by (2) using approximation (3) was not always stable at high frequencies near the model cutoff, and, as a safeguard, a limit on the increments of $F$ was imposed. The limiter introduced in the original version of the model was given by

$$|\Delta F|_{\max} = 6.4 \times 10^{-7}\, g^2 f^{-5}. \quad (7)$$

This limiter ensured that WAM remained numerically stable. However, as was shown by Tolman (1992), results for initial wave growth appeared to be quite sensitive to the choice of the time step. In contrast to reducing the model time step for initial wave growth, as was suggested by Tolman, it was found that the time

dependence could also be considerably reduced by choosing a limiter that is proportional to the time step:

$$|\Delta F|_{\max} = 6.4 \times 10^{-7} g^2 f^{-5} \Delta t/\tau, \qquad \tau = 1200 \text{ s}. \quad (8)$$

This limiter was introduced in the transition from cycle 3 to cycle 4 of WAM. The consequence of making the limiter proportional to the time step is that it will remain in the source term when the limit $\Delta t \to 0$ is taken. Therefore, in light of this, (8) is not just a numerical feature; it becomes part of the physics. Usually it is effective only for initial wave growth, in which the energy-containing part of the spectrum extends into the diagnostic high-frequency tail of the model spectrum, beyond the cutoff limiting the prognostic range of the model spectrum. Therefore, for initial wave growth, the limiter compensates for the lack of physics in the diagnostic part of the spectrum.

### b. Violation of scale invariance

For large-scale applications, such as the operational WAM at ECMWF (0.5° grid spacing), limiter (8) leads to satisfying results. The time-step dependence is largely reduced, and wave heights seem to scale according to the $u_*$ scaling discussed in the previous section. However, this limiter does not have the correct $u_*$ scaling properties. This can be seen most easily by rewriting (8) into dimensionless quantities:

$$|\Delta F^*|_{\max} = 6.4 \times 10^{-7} f^{*-5} \Delta t^* \left(\frac{u_*}{g\tau}\right), \quad (9)$$

in which the explicit appearance of $u_*$ violates the scale invariance. For instance, the ECMWF implementation ($\Delta X = 55$ km, $\Delta t = 15$ min) leads, for $U_{10} = 25$ m s$^{-1}$ ($u_* \sim 1.22$ m s$^{-1}$), to a comparable dimensionless situation as a WAM implementation on Lake George (a lake about 20 km × 10 km near Canberra, Australia) (Young and Verhagen 1997), with $\Delta X = 1.3$ km, $\Delta t = 2$ min (Hersbach 1998), and $U_{10} = 4$ m s$^{-1}$ ($u_* \sim 0.19$ m s$^{-1}$). Therefore, in this case the finite-difference schemes should be very similar; in particular, $|\Delta F^*|_{\max}$ should be comparable. However, the Lake George limiter (9), is more than six times as strict as the ECMWF implementation, which appears to result in a severe underprediction of wave height (about a factor of 2).

Therefore, in order to successfully implement WAM in small-scale applications, the limiter needs to be redefined in such a way that $u_*$ scaling is restored. In addition, the limiter should give rise only to a small time-step dependence, which is why limiter (7) is not a good candidate.

### c. Restoration of scale invariance

In the first WAM cycles, the limiter expressed the condition that the incremental change in the spectrum should not exceed a certain fraction of the Phillips (1958) universal equilibrium $f^{-5}$ spectrum. Later, it was found that for the intermediate spectral range beyond the energy-containing part of the spectrum this shape is not correct; the Toba spectrum is more appropriate. This has an $f^{-4}$ tail that scales with the friction velocity:

$$F_{\text{eq}} = \alpha_T g u_* f^{-4}. \quad (10)$$

The Toba spectral shape agrees with the WAM spectrum as implemented in cycle 4.

To obtain a correctly scaled limiter, the $u_*$ dependence of the high-frequency spectral level is considered and the constant timescale $\tau$ in (8) is replaced by a timescale defined by the model physics or numerics. This could be a relevant timescale of the wave spectrum (in which case the inverse of the mean frequency would be a candidate) or a relevant timescale of the numerical frequency grid—which would suggest the inverse of $f_c$ (the cutoff frequency) as a natural choice. It was found that $f_{\text{mean}}$ gives a somewhat smaller dependence on the time step for duration-limited growth curves but that $f_c$ gave more consistent results for fetch-limited growth curves at very small dimensionless fetches. Therefore, it is proposed that we replace (8) with

$$|\Delta F|_{\max} = 3.0 \times 10^{-7}\, g \tilde{u}_* f^{-4} f_c \Delta t, \quad (11)$$

in which $\tilde{u}_* = \max(u_*, g f^*_{\text{PM}}/f)$ and $f^*_{\text{PM}} = 5.6 \times 10^{-3}$ is the dimensionless Pierson–Moskowitz peak frequency. The inclusion of a minimum to $u_*$ anticipates windless situations. In this case, the limiter would reduce to zero, which means that swell dissipation would be prohibited. The validity of this minimum was checked by performing two windless runs: one with the minimum and one without. The run without the minimum showed no swell dissipation; the run with the minimum did. In addition, the limiter was never activated for the latter case. This gives us some confidence that $u^*_{\min} = g f^*_{\text{PM}}/f$ is a good choice. The scaling factor in (11) was chosen such that the limiter was restrictive as little as possible. On the basis of an extensive number of WAM runs for various temporal and spatial resolutions and for various frequency ranges and wind speeds, the value of $3.0 \times 10^{-7}$ was found to be suitable. In particular, WAM could now be successfully implemented for Lake George (Young and Verhagen 1997; Hersbach 1998). Limiter (11) is scale invariant because its scaled form depends only on scaled quantities:

$$|\Delta F^*|_{\max} = 3.0 \times 10^{-7} \max\left(1, \frac{f^*_{\text{PM}}}{f^*}\right) f^{*-4} f^*_c \Delta t^*.$$

It is noted that, in principle, several other limiter choices are possible. For example, one could choose a limiter that depends on $\sqrt{f_c \Delta t}$. This, in contrast to (11), has the advantage that the limitation does not enter the physics when the limit $\Delta t \to 0$ is made. The drawback, however, is that this appears to reintroduce a large time-step dependence on the initial wave growth, while (11) shows a much weaker sensitivity to the time step. In

testing the WAM model with limiter (11), it turned out that in certain circumstances numerical oscillations developed in the high-frequency part of the spectrum and in the friction velocity. These oscillations were suppressed by replacing the value $\alpha = ½$ for the implicit parameter $\alpha$ in (2) by $\alpha = 1$. Although this reduced the order of the scheme from 2 to 1, it was found to have a negligible impact on the integration. (The upwind advection scheme of the model is also only of first order.)

## 5. Experiments

### *a. Fetch-limited growth*

The essence of the promising performance of the new limiter (11) is given by the difference between Figs. 1 and 2. Figure 1 shows fetch-limited growth curves (i.e., dimensionless energy $\epsilon^* = g^2E/u_*^4$ and dimensionless peak frequency $f_p^* = u^* f_p/g$, versus dimensionless fetch $X^* = gX/u_*^2$) for three different wind speeds ($U_{10} = 10$, 20, 30 m s$^{-1}$) on the basis of the improved limiter (11). A grid consisting of 20 points in the downwind direction and one point in the direction perpendicular to the wind was used. Each grid point was chosen to be its own neighbor, in the latter direction, which mimics exactly the situation of an infinite coast line. Starting from a very low energy–containing initial spectrum, the model was integrated in time until a time-independent situation was reached. Three different spatial resolutions and frequency grids were used. In the first case (full lines), a grid resolution of 20 km was chosen, together with a frequency range from 0.04 to 0.4 Hz (corresponding to the normal operational WAM model). In the second case (dot–dashed curves), a much smaller grid resolution of 1 km was chosen. In these short fetches, the dominant part of the wave energy is found in the high frequencies, and therefore, a frequency range between 0.1 and 1 Hz was chosen. Finally, the dashed curves represent runs with a grid resolution of 167 km—that is, 1.5°, which was the grid distance used, until 1996, for the global model at the ECMWF. For the large wind speed $U_{10} =$ 30 m s$^{-1}$, the peak frequency reaches approximately 0.04 Hz. Therefore, a frequency range of 0.03–0.3 Hz was taken. The integration time for the three grids was 4 days for the 167-km grid, 1 day for the 20-km grid, and 6 h for the 1-km grid.

It is seen in Fig. 1 that all fetch curves join together to become one curve that very smoothly stretches over the entire fetch range $2 \times 10^3 < X^* < 2 \times 10^8$, that is, over five orders of magnitude. The only departures seen in these curves occur in the leveling at the beginning of the curves, which is caused by the first off-land point only. No significant dependence on the time step was found. Therefore, rather large time steps were used: 30 min for $\Delta X = 167$ km, 15 min for $\Delta X = 20$ km, and 2 min for $\Delta X = 1$ km.

The curves are reasonably close to the dotted curve, which represents an interpolation between the growth curves obtained by Kahma and Calkoen (1992) (on the basis of their composite dataset using a wave-state-dependent drag coefficient) for the moderate fetch range and the infinite fetch saturation values of Pierson and Moskowitz (1964):

$$\epsilon^* = 1.1 \times 10^3(1 + 9.51 \times 10^6/X^*)^{-0.96} \qquad (12)$$

and

$$f_p^* = 5.6 \times 10^{-3}(1 + 1.45 \times 10^7/X^*)^{0.29}.$$

If the strength of the WAM wind input source term was decreased by 10%, the match between curves (12) and the ''WAM'' curves would be excellent. Figure 2 shows results for exactly the same calculations but now using the original limiter (8). The deviation from a dimensionless fetch curve is seen to be dramatic for the small-scale grids. The curves for a grid distance of 1 km are much too low (by a factor as low as 10) because the limiter (8) is much too restrictive, as indicated in the bottom panel in Fig. 2. The violation in $u_*$ scaling is seen most clearly in the difference between the $U_{10} =$ 30 m s$^{-1}$ run for a grid resolution of 20 km and the $U_{10}$ $= 10$ m s$^{-1}$ run for a grid resolution of 1 km. Both runs correspond to the same dimensionless fetch range $X^*$ $\sim 10^5$–$10^6$. Although for the new limiter (11) both curves are very close, the original limiter (8) curves are widely separated.

So far, nondimensional quantities have been compared. In practice, one is interested in unscaled quantities. Since the wave energy scales with $u_*^4$, a small deviation in $u_*$ implies a large change in $E$. To investigate whether the improved limiter has a real impact on unscaled wave heights as well and is not simply an effect of a modification in $u_*$ (which in WAM cycle 4 depends on the sea state), Fig. 3 shows a plot of the significant wave height versus the fetch. The left panel shows the results for runs with a grid resolution of 20 km and a wind speed of $U_{10} = 30$ m s$^{-1}$. The right panel shows the corresponding results for a grid resolution of 1 km and $U_{10} = 10$ m s$^{-1}$. Both runs correspond to comparable dimensionless fetch ranges, and the growth curves should therefore be similar in shape. This is approximately true for the new limiter, although the curve for the 20-km run is somewhat flatter than the 1-km run. This is because the peak frequency for $U_{10}$ $= 30$ m s$^{-1}$ approaches the minimum frequency of 0.04 Hz for the fetch range of this run. If a lower minimum frequency were used, the resemblance between the 1- and 20-km curves would become excellent. In contrast, the wave heights of the 1-km run for the original integration scheme are about 50% too low. Thus it is seen that the scaling violation of the old limiter has serious implications for small spatial scales.

### *b. Duration-limited growth*

The impact of limiter (11) on duration-limited growth is illustrated in Figs. 4 and 5. These figures

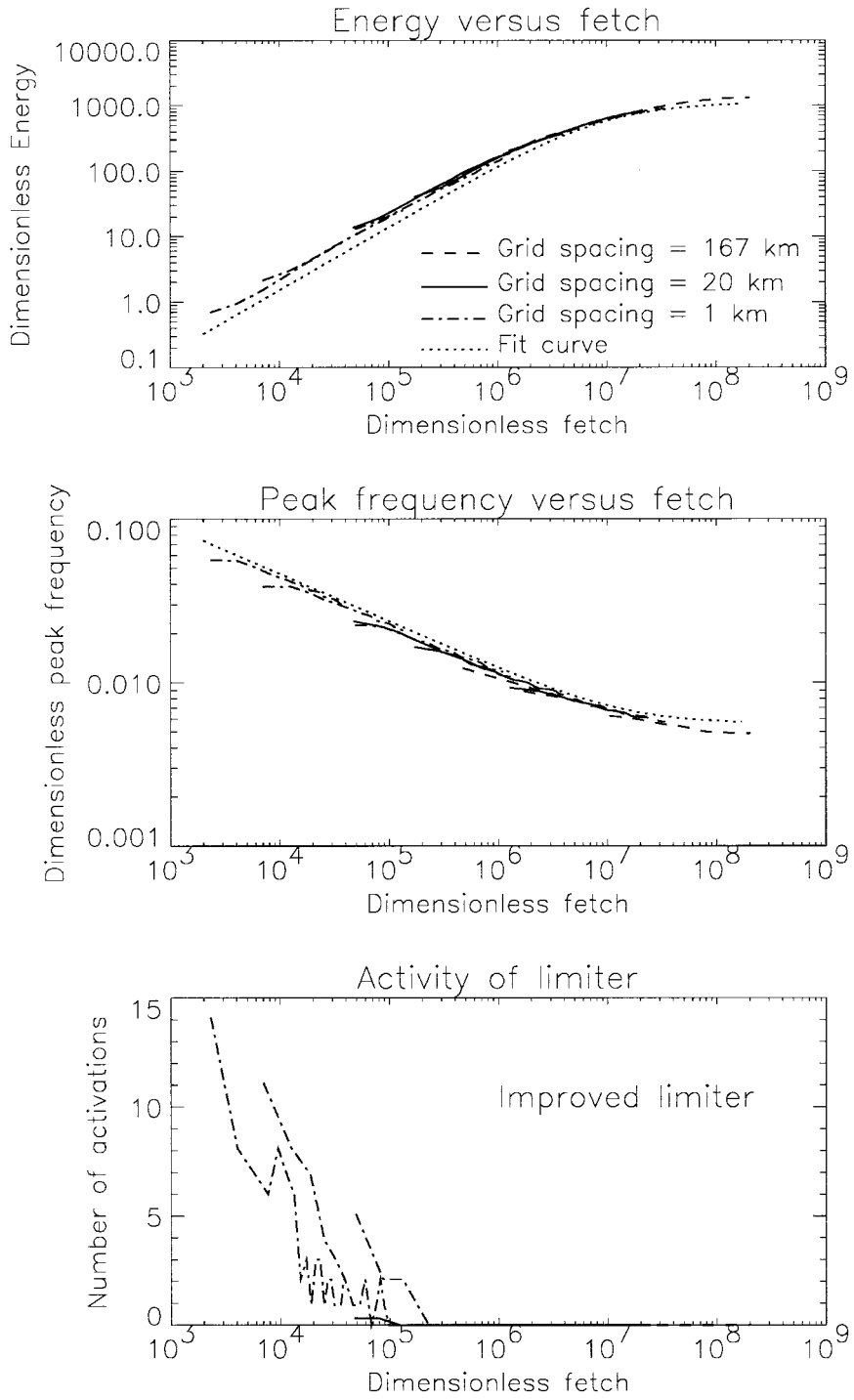


FIG. 1. Fetch-limited growth curves in dimensionless quantities, obtained with the newly proposed integration scheme and limiter (11). Runs for three different resolutions, 167, 20, and 1 km, were performed, each for three different wind speeds $U_{10}$ = 10, 20, and 30 m s$^{-1}$. The experimental curve (dotted) is defined by (12).

show, for the old (Fig. 4) and new limiter (Fig. 5), the duration-limited evolution of the significant wave height, peak frequency, and friction velocity for a 25 m s$^{-1}$ wind speed. Also shown are the number of spectral bins at which the limiter was active (counted over the 25 frequencies times 12 directions; usually the activations occur in the higher-frequency bins located around the wind direction). Runs were performed for

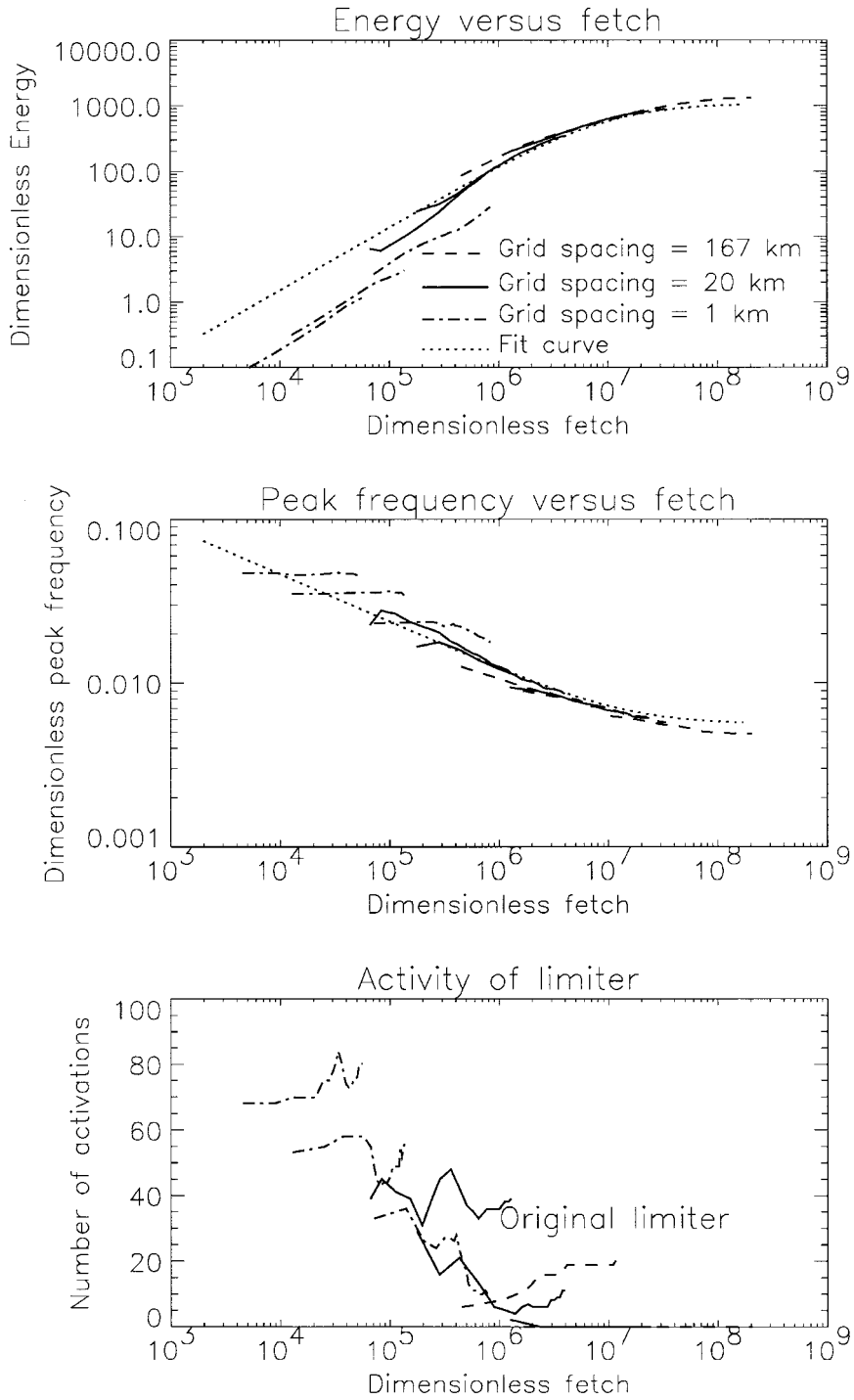


FIG. 2. Fetch-limited growth curves in dimensionless quantities, obtained with the default WAM cycle 4 integration scheme. Runs for three different resolutions, 167, 20, and 1 km, were performed, each for three different wind speeds $U_{10} = 10$, 20, and 30 m s$^{-1}$. The experimental curve (dotted) is defined by (12).

time steps of 1200, 600, and 1 s. The 1-s runs can be regarded as the limit $\Delta T \to 0$, in which $(|\Delta F|_{\max}/\Delta T)$ becomes part of the source term $S$. For both cases it is seen that for significant wave height and peak frequency the convergence to this limit is quite fast. Only for the 1200-s run is there a noticeable difference. The run with $\Delta T = 600$ s is already very close to the continuity limit. The convergence for friction velocity

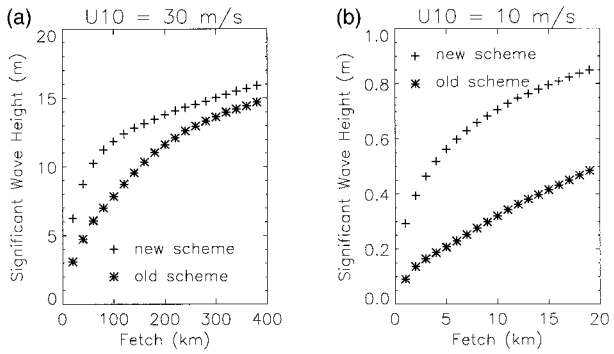


FIG. 3. Fetch-limited growth curves in unscaled quantities. (a) Results for runs with a grid resolution of 20 km and a wind speed of 30 m $s_{-1}$. (b) Results for a resolution of 1 km and $U^{10} = 10$ m $s^{-1}$.

(which depends on the sea state in cycle 4 of WAM) is slower.

In addition, runs were performed that were based on limiters that did not contribute to $S$ for $\Delta T \to 0$, such as (7) or a limiter that is proportional to $\sqrt{\Delta T}$. In all of these cases, a much larger dependence on the time step was found (not displayed). The reason for this may be that the time-step dependence is reduced mainly after the number of spectral bins, at which the limiter is active, has converged. This number can be zero, which is the case for limiters that vanish in the limit $\Delta t \to 0$. However, in certain situations (such as initial wave growth) the time step at which this point is reached may be quite small, resulting in a large dependence in the operationally feasible range of time steps. The solution to get around this problem is to reduce the time step whenever that is necessary (Tolman 1992). Alternatively, this number may be larger than zero, which can be the case for a limiter that does enter the physics, such as limiter (11). Convergence to that number (which value depends on the situation and therefore on time) is achieved for time steps that are quite large. For limiter (11) this is indeed true, as can be seen in the lower right panel of Fig. 5: the curves for all time steps used are right on top of each other.

Also shown in Figs. 4 and 5 (solid lines) are the results of a run with a time step of 1 s in which no limit on maximal wave growth per time step was applied. This run can be regarded as the limit $\Delta T \to 0$, without the inclusion of an extra term in $S$. From this run the impact of the limiter can be revealed. For the original limiter, the effect appears to be very large. The initial wave growth is highly suppressed and results in a time lag for later times. This is also illustrated in the lower right panel of Fig. 4, which shows that limiter (8) is very active.

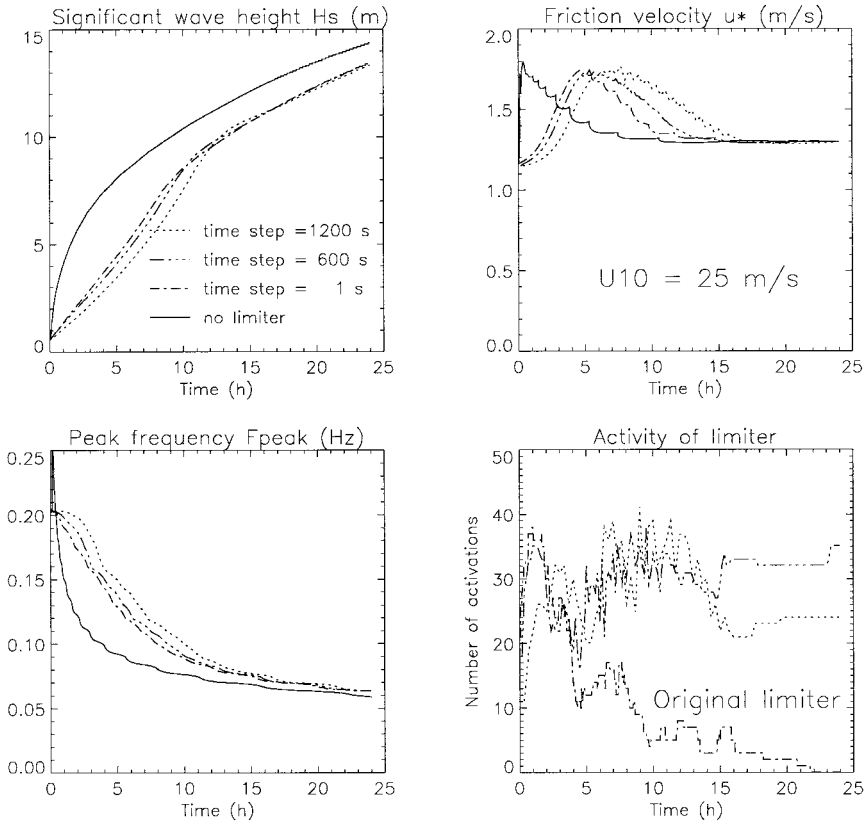


FIG. 4. Duration-limited evolution for wave height, peak frequency, and friction velocity, using the default WAM cycle 4 model, that is, the semi-implicit scheme (2) with $\alpha = ½$.

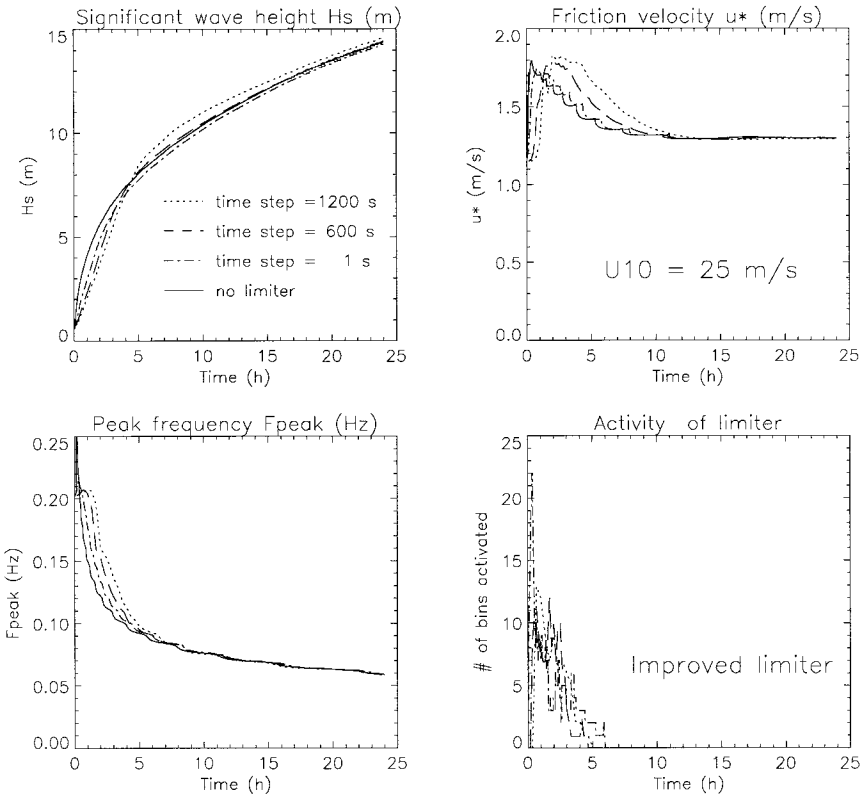


FIG. 5. Duration-limited evolution for wave height, peak frequency, and friction velocity, using the newly proposed scheme, that is, $\alpha = 1$ in (2) and limiter (11).

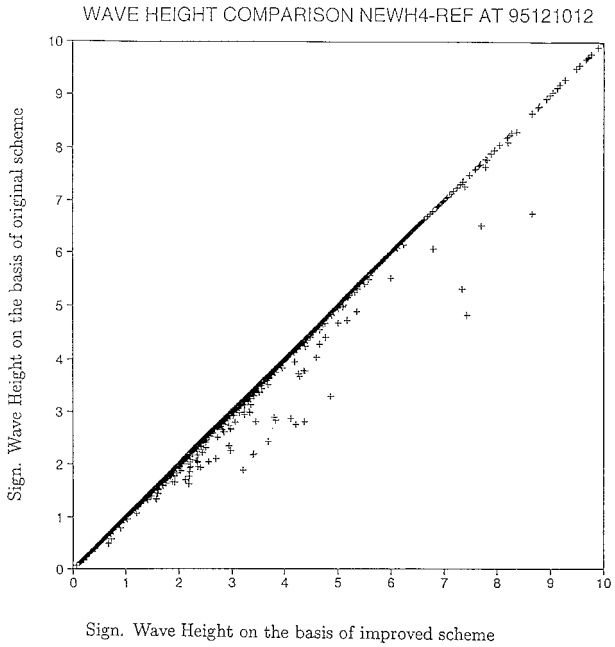


FIG. 6. Scatterplot of the significant wave height resulting from a 10-day global run of WAM at ECMWF on the basis of the original scheme vs the significant wave height obtained using the improved scheme.

On the other hand, the impact of the newly proposed limiter (11) is very modest. Only the first few hours' wave growth is somewhat slower. Only at this initial stage is limiter (11) active (but much less so than the original limiter), as can be seen in the lower right panel of Fig. 5. There is practically no time lag. The difference between both curves may be well within the experimentally known accuracy.

### *c. The WAM model at ECMWF*

Finally, we investigated whether these errors have significant implications for the scales relevant for normal operational wave forecasting. WAM was run with limiter (11) on analyzed winds for a 10-day period (starting at 12 h GMT, 5 December 1995), and the results were compared to the WAM version that was operational at ECMWF on 5 December 1995. Both versions had 12 directions, 25 frequencies (between 0.04 and 0.4 Hz), and a spatial resolution of 1.5°. The propagation time step was 30 min, and the integration time step was 15 min. Figure 6, which displays a scatter diagram for wave height, and Fig. 7, which shows a wave-height difference field, indicate that differences are indeed occasionally found. However, the differences are local (e.g., the fetch-limited case near the East Coast of the

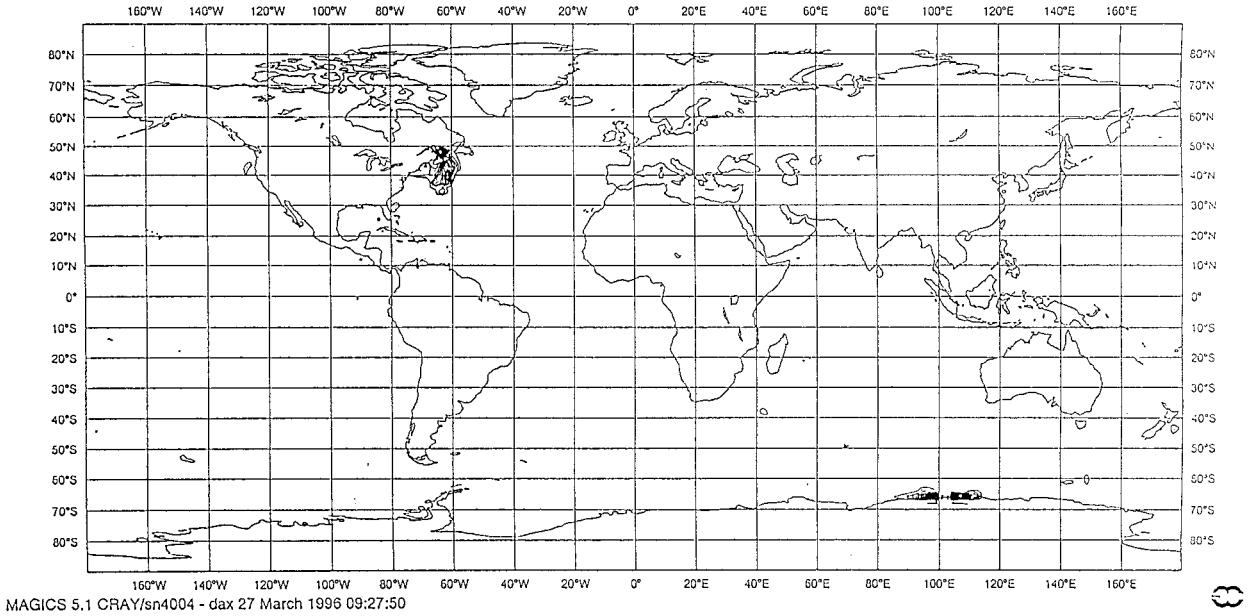


FIG. 7. Difference plot between the significant wave height resulting from a 10-day global run of WAM at ECMWF (starting at 12 h GMT on 5 December 1995) on the basis of the original scheme and the significant wave height obtained using the improved scheme.

United States), although they can be as much as 2 m in wave height.

## 6. Conclusions

To summarize, a new limiter, (11), that is consistent with friction velocity scaling was introduced to the WAM integration scheme. Using a fully implicit integration scheme (2) with $\alpha = 1$, results were obtained that are free of numerical noise and that scale correctly, independent of grid resolution and the time step, even in extreme conditions of very small dimensionless fetches.

The WAM model, using limiter (11), has been successfully implemented for Lake George [Hersbach (1998); for a description of the experimental setup up, see Young and Verhagen (1997)]. The necessary updates to WAM can be obtained by contacting the corresponding author.

*Acknowledgments.* This work was carried out as part of the European Coupled Atmosphere/Wave/Ocean-Model (ECAWOM) project, funded by the MAST (Marine Science and Technology) Programme of the European Union. We are grateful to K. Hasselmann and G. Komen for helpful discussions and constructive comments on a first draft of this paper.

REFERENCES

Hersbach, H., 1998: Application of the adjoint of the WAM model to inverse wave modeling. *J. Geophys. Res,* **103,** 10 469–10 487.

Janssen, P. A. E. M., and J. D. Doyle, 1997: On spurious chaotic behaviour in the discretized ECMWF physics scheme. ECMWF Tech. Memo. 234, 24 pp. [Available from ECMWF, Shinfield Park, Reading RG2 9AX, United Kingdom.]

Kahma, K. K., and C. J. Calkoen, 1992: Reconciling discrepancies in the observed growth of wind-generated waves. *J. Phys. Oceanogr.,* **22,** 1389–1405.

Komen, G. J., L. Calaleri, M. Donelan, K. Hasselmann, S. Hasselmann, and P. A. E. M. Janssen, 1994: *Dynamics and Modelling of Ocean Waves.* 1st ed. Cambridge University Press, 532 pp.

Phillips, O. M., 1958: The equilibrium range in the spectrum of wind-generated water waves. *J. Fluid Mech.,* **4,** 426–434.

Pierson, W. J., Jr., and L. Moskowitz, 1964: A proposed spectral form for fully developed wind seas based on the similarity theory of S. A. Kitaigorodskii. *J. Geophys. Res.,* **69,** 5181–5203.

Tolman, L., 1992: Effects of numerics on the physics in a third-generation wind-wave model. *J. Phys. Oceanogr.,* **22,** 1095–1111.

WAMDI, 1988: The WAM model—A third-generation ocean wave prediction model. *J. Phys. Oceanogr.,* **18,** 1775–1810.

Young, I., L. A. Verhagen, and S. K. Khatri, 1996: The growth of fetch-limited waves in water of finite depth: Parts I and II. *Coastal Eng.,* **29,** 47–100.